Critical and multicritical behavior in a triangular-lattice-gas Ising model: Repulsive nearest-neighbor and attractive next-nearest-neighbor coupling

D. P. Landau
Department of Physics and Astronomy, University of Georgia, Athens, Georgia 30602
(Received 20 December 1982)

Monte Carlo simulations have been used to study a triangular lattice-gas (Ising) model with repulsive nearest-neighbor interactions and attractive next-nearest-neighbor coupling. We find two ordered $(\sqrt{3}\times\sqrt{3})$ phases (one with $\frac{1}{3}$ of the sites occupied and one with $\frac{2}{3}$ of the sites filled). These ordered phases are separated from the disordered state by a phase boundary which is second order at high temperatures and which has tricritical points and first-order transitions at low temperatures. The critical and tricritical exponents are consistent with those predicted for the three-state Potts model. At 50% coverage we find a low-temperature ordered phase which is separated from the disordered state by an *XY*-like line of critical points which exist between upper and lower temperatures T_1 and T_2, respectively. Along this line between T_1 and T_2 we find nonuniversal critical behavior and identify topological (vortexlike) excitations.

I. INTRODUCTION

The triangular Ising antiferromagnet, which is equivalent to a triangular-lattice-gas model by an exact transformation,[1] has been of considerable interest ever since it was shown that in zero field there is no transition to an ordered state at any finite temperature.[2] Further studies[3,4] have shown that an ordered ferromagnetic, or $(\sqrt{3}\times\sqrt{3})$-lattice-gas, phase[5] exists in nonzero magnetic field, or chemical potential (see Fig. 1). Campbell and Schick[6] used a Bethe-Peierls-Weiss approximation to study the phase transitions which occur when next-nearest-neighbor attraction was added so as to make the model appropriate for the description of physical adsorption of gases on graphite.[7,8] The results of this calculation showed two ordered phases, $(\sqrt{3}\times\sqrt{3})$ and $(\sqrt{3}\times\sqrt{3})^*$, existing in regions clearly separated in chemical-potential temperature space and undergoing first-order transitions to the disordered state. Alexander,[9] however, used symmetry arguments to predict that the phase transition between the ordered and disordered state should belong to the universality class of the three-state Potts model. The same result was obtained independently using a group theory analysis.[10] Mihura and Landau[11] studied this same model using a Monte Carlo method and obtained a very different phase diagram from Campbell and Schick. They found instead [see Fig. 1(b)] that the two phases coexist over a wide range of temperature and that each phase is indeed separated from the disordered state by a line of second-order transitions which becomes first order only at temperatures below a tricritical point. They did not, however examine the critical behavior in detail. The phase transition behavior is expected to be particularly interesting in zero field where the $(\sqrt{3}\times\sqrt{3})$ and $(\sqrt{3}\times\sqrt{3})^*$ states become degenerate. This "degenerate" state has been predicted[10] to be in the universality class of the *XY* model with

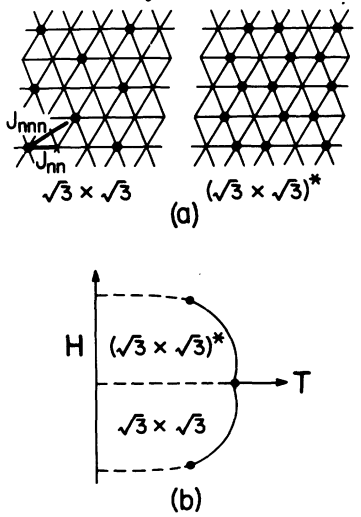

FIG. 1. (a) Ordered $(\sqrt{3}\times\sqrt{3})$-type states for the triangular-lattice-gas model. Filled circles represent adatoms. Nearest-neighbor coupling (J_{NN}) and next-nearest-neighbor coupling (J_{NNN}) are shown on the left. (b) Schematic phase diagram for $R=-1$, taken from Ref. 11.

sixth-order anisotropy.[12] This latter model is expected to have interesting behavior with a low-temperature ordered phase separated from the disordered phase by an intermediate XY-like state. A low-temperature study of a generalized Villain model suggests that a low-temperature ordered phase is separated from the high-temperature disordered state by an intermediate XY-like state. (This behavior is similar to that obtained from series expansions for the Z_p model.[13]) However, a numerical study[12] of the Migdal recursion relations for this model contradicts this prediction since it shows no such behavior.

The purpose of this work is to provide a careful study not only of the location of phase boundaries and multicritical points but also of critical behavior. In Sec. II we review relevant theoretical background, and we present our results in Sec. III. [We shall see there that indeed the phase diagram shown in Fig. 1(b) misses one crucial feature at $H=0$.]

II. THEORETICAL BACKGROUND

A. The model

The next-nearest-neighbor (NNN) triangular Ising model is described by the Hamiltonian

$$\mathcal{H}=J_{\mathrm{NN}}\sum_{\mathrm{NN}}\sigma_i\sigma_j+J_{\mathrm{NNN}}\sum_{\mathrm{NNN}}\sigma_i\sigma_k+H\sum\sigma_i\ , \quad (1)$$

where $\sigma_i,\sigma_j,\sigma_k=\pm1$, J_{NN} and J_{NNN} are NN- and NNN-coupling constants, respectively, H is a uniform magnetic field, and the sums run over the indicated pairs of neighbors on a triangular lattice. We define the ratio of interactions by $R=J_{\mathrm{NNN}}/J_{\mathrm{NN}}$. This magnetic model can also be related[14] to a lattice-gas model which is appropriate to adatom adsorption on periodic substrates. For the lattice-gas model we define site-occupation variables c_i where $c_i=1$ if site i is occupied and $c_i=0$ if site i is empty. If binding energy ϵ is gained when an adatom is adsorbed and adatoms interact with site-site coupling ϕ, the lattice-gas Hamiltonian can be written

$$\mathcal{H}-\mu N_a=-\tfrac{1}{2}\sum_{i\neq j}c_ic_j\phi(\vec{r}_i-\vec{r}_j)-(\epsilon+\mu)\sum_i c_i+H_0\ , \quad (2)$$

where μ is the chemical potential, N_a is the total number of adsorbed atoms, and H_0 describes other degrees of freedom. Using the simple transformation

$$c_i=(1-\sigma_i)/2\ , \quad (3)$$

we find that Eq. (2) becomes identical to Eq. (1) with

$$J_{\mathrm{NN}}=\phi_{\mathrm{NN}}/4\ , \quad (4a)$$

$$J_{\mathrm{NNN}}=\phi_{\mathrm{NNN}}/4\ , \quad (4b)$$

$$H=-(\epsilon+\mu+3\phi_{\mathrm{NN}}+3\phi_{\mathrm{NNN}})\ , \quad (4c)$$

where we have set all couplings between sites farther apart than next nearest neighbors equal to zero and have explicitly included the fact that there are six NN sites and six NNN sites for the triangular lattice. The magnetization of the Ising model

$$M=\frac{1}{N}\sum_i\sigma_i \quad (5)$$

is then simply related to the coverage of the lattice-gas model

$$\theta=\frac{1}{N}\sum_i c_i \quad (6)$$

by

$$\theta=(1-M)/2\ . \quad (7)$$

The Ising model in zero field has zero magnetization (because of time-reversal symmetry) and the corresponding lattice-gas model is therefore one with coverage $\theta=\frac{1}{2}$ [see Eq. (7)].

The ordered states shown in Fig. 1 can best be described by decomposing the original lattice into three interpenetrating sublattices made up of sites connected by NNN bonds. (Each sublattice now has a lattice constant equal to $\sqrt{3}$ times that of the original lattice.) The $(\sqrt{3}\times\sqrt{3})$ ordered state corresponds to one sublattice filled and the other two empty. Since all three sublattices are equivalent, this state is threefold degenerate. In the $(\sqrt{3}\times\sqrt{3})^*$ state one sublattice is empty and the other two filled; this state is also threefold degenerate. In terms of the sublattice magnetizations

$$M_\alpha=\frac{3}{N}\sum_{i\in\alpha}\sigma_i,\quad \alpha=1,2,3 \quad (8)$$

we can define three order parameters

$$m_1=\left|M_1-\left|\frac{M_2+M_3}{2}\right|\right|\Big/2\ , \quad (9a)$$

$$m_2=\left|M_2-\left|\frac{M_1+M_3}{2}\right|\right|\Big/2\ , \quad (9b)$$

$$m_3=\left|M_3-\left|\frac{M_1+M_2}{2}\right|\right|\Big/2\ , \quad (9c)$$

with a corresponding root-mean-square order parameter

$$m=\frac{\sqrt{6}}{3}(m_1^2+m_2^2+m_3^2)^{1/2} . \quad (10)$$

This definition of order parameters is computationally convenient although there can be only two independent order parameters. Clearly an equivalent lattice-gas order parameter can be defined in terms of sublattice occupancies.

B. Finite-size scaling

We have studied $L\times L$ lattices with periodic boundary conditions applied so as to remove edge effects. (Although the free-edge condition might be more appropriate for comparison with experimental results on physical systems, the use of periodic boundary conditions yields results which are less affected by finite lattice size.) The behavior of finite systems near the critical temperature of the corresponding infinite system can be described by finite-size scaling theory.[15–18] If the infinite system has the usual power-law singularities, with critical exponents α,β,γ,ν, etc., the behavior of the finite $L\times L$ system is expressed in terms of a scaled temperature $x=tL^{1/\nu}$ where $t=|1-T/T_c|$. Thus near T_c for sufficiently large L we can write finite-size scaling expressions,

$$m=L^{-\beta/\nu}\bar{X}(x)\approx Bt^{\beta} \text{ as } L\to\infty , \quad (11a)$$

$$\chi T=L^{\gamma/\nu}\bar{Y}(x)\approx Ct^{-\gamma} \text{ as } L\to\infty , \quad (11b)$$

$$C-C_0=L^{\alpha/\nu}\bar{Z}(x)\approx At^{-\alpha} \text{ as } L\to\infty , \quad (11c)$$

where C_0 is the nondivergent "background" contribution to the specific heat. In addition, the site-site correlation scales as a function of two variables $x=tL^{1/\nu}$ and $y=r/L$:

$$\langle\sigma_i\sigma_j\rangle\approx r^{-\eta}\mathcal{F}(x,y) \text{ as } r,L\to\infty . \quad (12)$$

In the case of exponential singularities, such as the Kosterlitz-Thouless form[19] where the correlation length diverges as

$$\xi=\xi_0\exp(at^{-1/2}) \quad (13)$$

instead of as $t^{-\nu}$, finite-size scaling can be extended by using ξ/L as the scaling variable. This means, for example, that

$$m\approx L^{-b}\tilde{\bar{X}}[L^{-1}\exp(at^{-1/2})] \text{ as } r,L\to\infty \quad (14a)$$

$$\chi T\approx L^{c}\tilde{\bar{Y}}[L^{-1}\exp(at^{-1/2})] \text{ as } r,L\to\infty . \quad (14b)$$

C. Monte Carlo method

We have used a standard importance sampling Monte Carlo method which has been described in detail elsewhere.[18,20,21] We studied $L\times L$ lattices with periodic boundary conditions for $12\le L\le 90$. Between 100 MCS/s (Monte Carlo steps/site) and 500 MCS/s were first discarded and then 1000–5000 MCS/s were retained for computing averages. Each data point was repeated at least once using a different starting configuration. Lattice configurations were also printed out so that we could look for domains and other topological configurations. Because the order parameter as we define it is positive for all possible states, we define the ordering susceptibility as

$$\chi^{+}=\frac{N}{T}\langle m^2\rangle , \quad (15)$$

where m is the order parameter defined by Eq. (10) and $N=L^2$ is the total number of sites.

III. RESULTS AND DISCUSSIONS

A. The degenerate state

1. Bulk properties for $R=-1$

As mentioned earlier for $\theta=\frac{1}{2}$, i.e., $H=0$, all six ground states are degenerate. The zero-field specific-heat data for the case where the repulsive NN coupling and attractive NNN interactions are the same in magnitude, i.e., $R=J_{\mathrm{NNN}}/J_{\mathrm{NN}}=-1$, are shown in Fig. 2. Two clearly separated, rounded peaks are observed; the magnitudes of the maxima very quickly become size independent. In Fig. 3 we show the variation of the order parameter with tem-

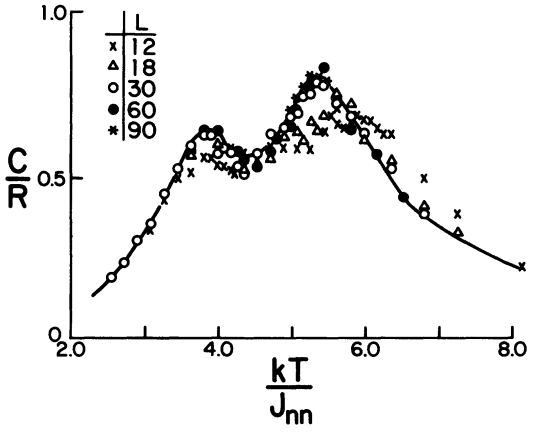

FIG. 2. Specific heat vs temperature in zero field for $R=-1$. The solid curve shows the estimated infinite-lattice behavior.

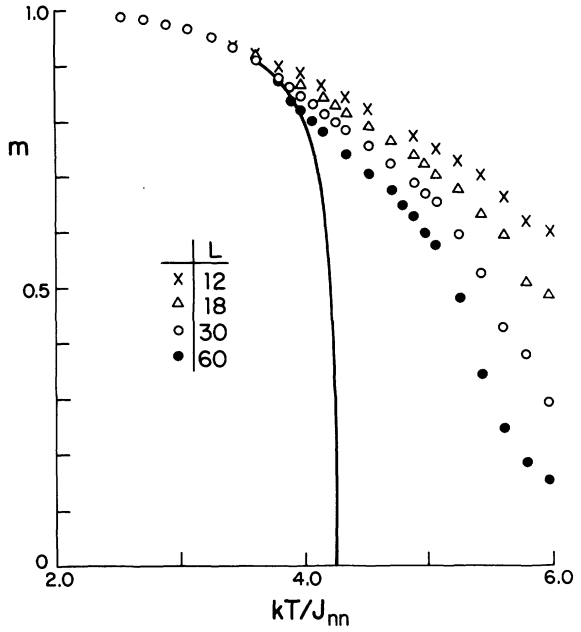

FIG. 3. Temperature dependence of the order parameter in zero field for $R=-1$. The solid curve shows the extrapolated infinite-lattice behavior.

perature. In qualitative terms we see three regions with different finite-size behavior. Below $kT/J_{NN}\sim 4$ the effects of finite size are quite small, and above $kT/J_{NN}\sim 5$ the order parameter decreases rapidly with increasing lattice size. In the intermediate region the order parameter falls off rather slowly with increasing L. Since the magnetization will average out to zero if all states are sampled, it was not possible to determine the temperature dependence from long runs at $H=0$. Instead,

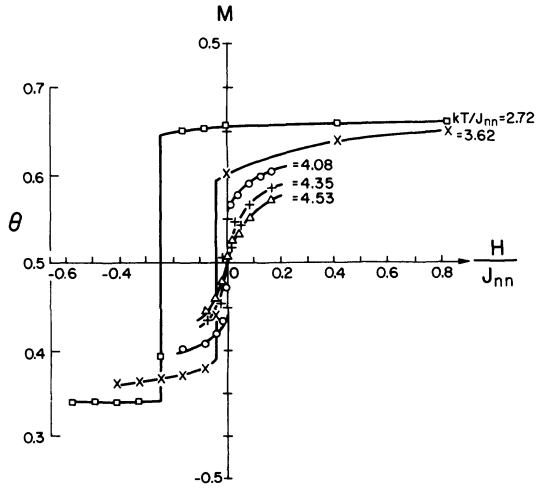

FIG. 4. Field dependence of the coverage (magnetization) along isotherms for $R=-1$.

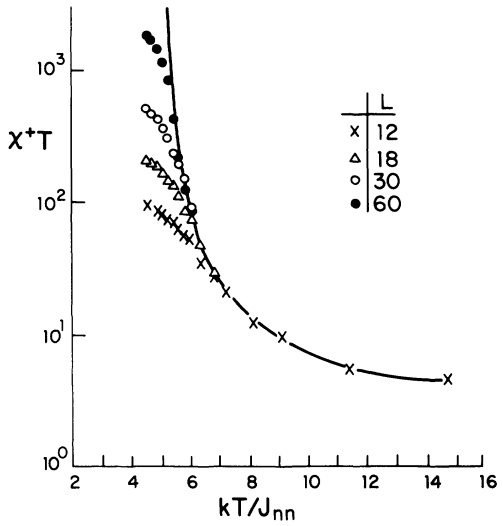

FIG. 5. High-temperature ordering susceptibility in zero field for $R=-1$. The solid curve shows the extrapolated infinite-lattice behavior.

the behavior of the magnetization in the degenerate state [or coverage $\theta=(1-M)/2$] was determined through isothermal field sweeps. The results, shown in Fig. 4, showed clear evidence of metastability at low temperature; pronounced hysteresis was observed. (These results are symmetric about $H=0$ and we only show data for the field being swept in one direction so as not to confuse the figure.) As the temperature increases, the discontinuity at $H=0$ decreases and disappears at $kT/J_{NN}=4.26$. For higher temperatures the slope at $H=0$ (dM/dH is the ordinary susceptibility) continuously decreases. The high-temperature ordering susceptibility data are shown in Fig. 5. The ordering susceptibility diverges rapidly and shows pronounced finite-size rounding as the temperature is decreased.

2. *Critical behavior for $R=-1$*

We have relied heavily on finite-size scaling analyses to extract critical behavior from our data. In Fig. 6 we plot the maximum value of the specific heat versus lattice size. For comparison we also show the size variation of the specific-heat peak for the triangular Ising ferromagnet which has a logarithmic ($\alpha=0$) divergence. The peak value for our model is clearly nondivergent; it does not increase for $L>30$ and the specific-heat exponent $\alpha<0$.

The finite-size behavior of the order parameter and ordering susceptibility could not be fitted to the usual scaling forms, e.g., Eq. (11). The reason for this became clear when we examined the critical behavior of the inverse correlation length. The

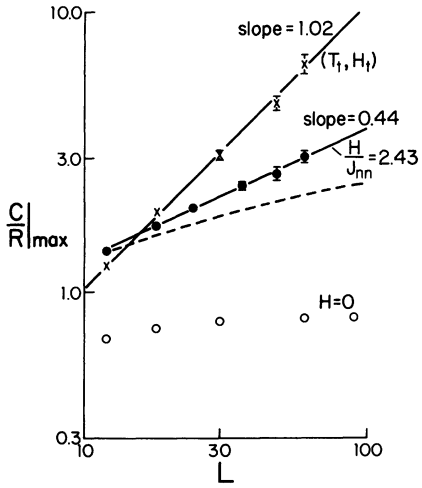

FIG. 6. Size dependence of the specific-heat maximum for $R=-1$ along different paths. The dashed curve shows the results for the NN-triangular ferromagnet.

correlation functions in the NNN direction (i.e., sites on the same sublattice) were averaged over the three equivalent directions and then analyzed assuming an Ornstein-Zernike form:

$$\langle \sigma_i \sigma_j \rangle - \langle \sigma_i \rangle^2 = \frac{De^{-\kappa r}}{r^{1/2}} , \tag{16}$$

where κ is the inverse correlation length and the averages $\langle\ \rangle$ are over sites in a single sublattice. For $T > T_c$, $\langle \sigma_i \rangle = 0$. (The sign of the NN correlation is

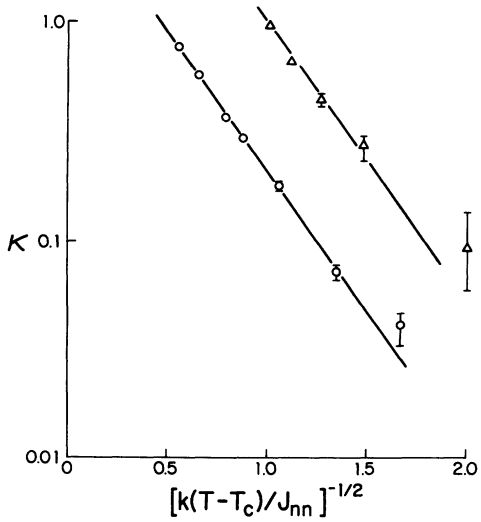

FIG. 7. Temperature dependence of the inverse correlation length in zero field for $R=-1$. Circles are data for $T > T_c = T_1$ and triangles are for $T < T_c = T_2$. κ is in units of the inverse NNN distance r_{NNN}^{-1}.

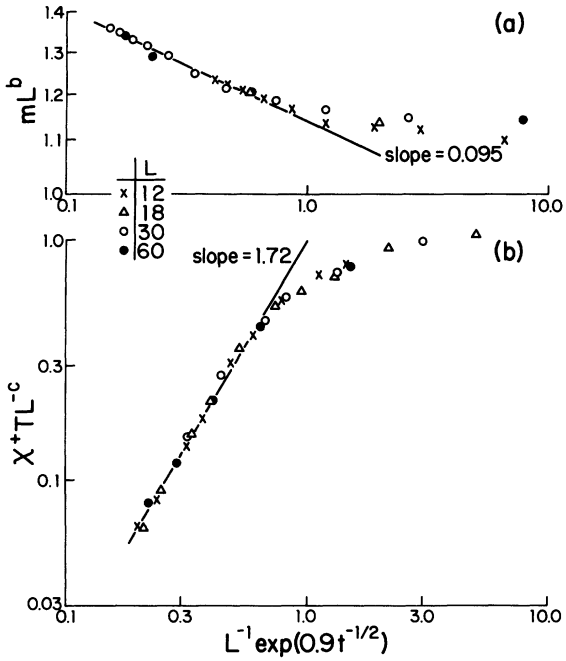

FIG. 8. Finite-size scaling plots in zero field for $R=-1$: (a) order parameter with $b=0.095$; (b) high-temperature ordering susceptibility with $c=1.72$.

sublattice dependent whereas the NNN correlation is independent of the sublattice.) We found that the inverse correlation length goes to zero exponentially fast (see Fig. 7) from above and below but that there are two critical temperatures, i.e., κ goes to zero at different temperatures when "T_c" is approached from above and below. Since this behavior means that the correlation length diverges exponentially fast, we used the modified finite-size scaling form described by Eq. (14) to analyze the order parameter and ordering susceptibility. As shown in Fig. 8, both quantities scale extremely well with $T_c = T_1 = 4.89 J_{NN}/k$ for the high-temperature ordering susceptibility and $T_c = T_2 = 4.26 J_{NN}/k$ for the order parameter. From Eq. (12) we see that the site-site correlations should scale as a function of two variables. If we are at T_c, however, one scaling variable ($x = tL^{1/\nu}$) becomes zero and the scaling function depends only upon the other variable $y = r/L$.

We have analyzed the finite-size behavior of the site-site correlation function in Fig. 9. The errors in the correlations are less than the size of the data points. Of course, due to the periodic boundary conditions it is not possible to obtain values for the correlations at distances $r \geq L/2$. We find that for all temperatures between T_1 and T_2 the data scale as a function of a single variable but using a value of η which depends continuously upon temperature (see

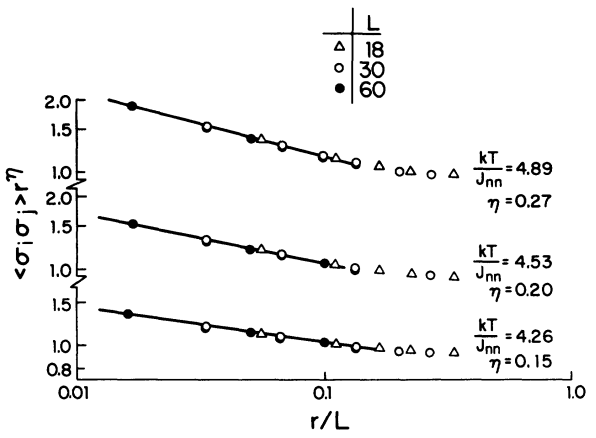

FIG. 9. Finite-size scaling plots for the site-site correlations for $R=-1$. Data are in units of r_{NNN} (NNN distance).

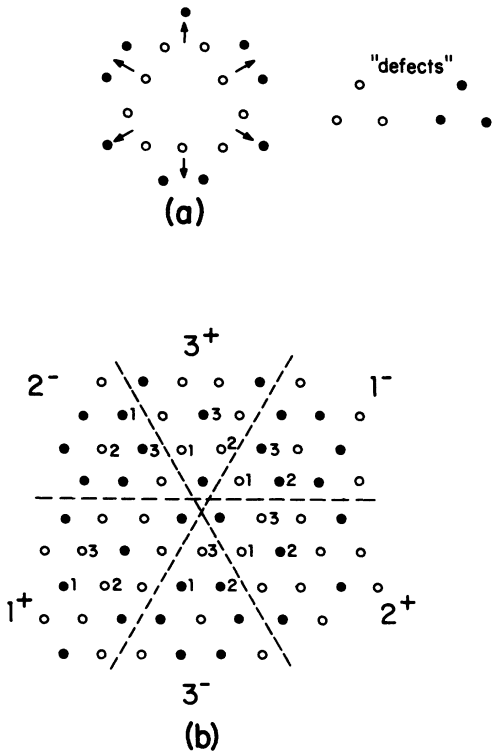

FIG. 10. (a) Vector notation for the six different "ground-state" NN triangles. The "defect" triangles cannot exist in the ground state. (b) "Vortex" configuration with dashed lines separating domains of different ground states. Sites are labeled by sublattice (i.e., 1, 2, or 3). Each domain is labeled by a number which denotes the "minority" sublattice and a + or − superscript which indicates that the "minority" sublattice is full or empty, respectively.

Fig. 9) and is thus nonuniversal. This means that every temperature between T_1 and T_2 is a critical point. Our estimates are $\eta=0.27\pm0.02$ at T_1 and $\eta=0.15\pm0.02$ at T_2. These values are close to the theoretical predictions[12] of $\eta=\frac{1}{4}$ at T_1 to $\eta=\frac{1}{9}$ at T_2. (We do not know if the small discrepancy at T_2 is due to incorrect location of T_2 and/or statistical error, or if it is real and due to an inadequacy of the theory.)

Since the bulk properties are consistent with XY-like behavior, it would be desirable to complete the picture with a description of topological excitations which play a role equivalent to vortices in the Kosterlitz-Thouless picture of the XY model.[19] Excitations from the ground state are easy to produce. For example, the removal of one adatom or the filling of an empty site (i.e., single spin flips in magnetic language) are simple elementary excitations. Such excitations only affect the lattice locally; far from the excitation the lattice is still in the ground state. We will attempt to describe "vortexlike" excitations with the aid of Fig. 10. In Fig. 10(a) we show six NN triangles each of which is in one of the six degenerate ground states. We develop a simple schematic representation in which an arrow in the center of each triangle points towards the occupied site; in the case of two occupied sites the arrow points halfway between the two occupied sites. Note that if we integrate the phase angle between arrows about the hexagonal path through the arrows, we obtain a circulation $\phi=2\pi$. These "vortices" are "stiff" in that the arrows cannot rotate freely to produce minor changes in vortex shape and core energy. Note that the only possible NN triangle states not included are the "defect states" in which all sites are either occupied or filled. In Fig. 10(b) we show the lattice when sites not shown in Fig. 10(a) are considered; the three sublattices are numbered in the central part of the lattice. Note that the lattice has now been broken up into six domains each of which is in one of the six degenerate ground states. For purposes of further discussion we assume the stability of the six independent domains. We expect, however, that at finite temperatures the picture shown in Fig. 10(a) will be somewhat distorted due to the presence of other excitations. Each domain is labeled by a number which identifies the minority sublattice and by a + if that minority sublattice is filled and a − if that sublattice is empty. Note that this topological configuration cannot repair itself *locally* and that an isolated "defect" (in this case all sites filled) is at the center. This topological excitation corresponds to a vortex in the XY model. If we create a similar configuration nearby in which the order of the appearance of domains is reversed as we move about the center in the clockwise direction, we

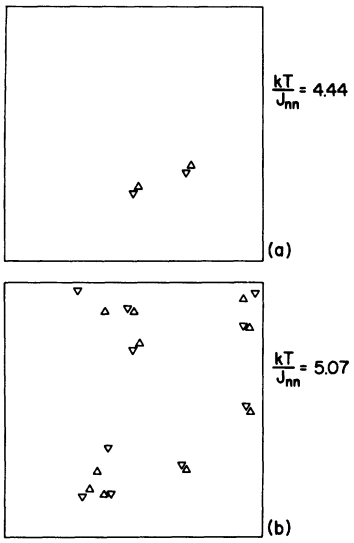

FIG. 11. Representation of the lattice showing only isolated defect triangles (vortex cores) for $R=-1$ in zero field. The lattices shown are 60×60.

find another defect in the center but one whose vertex points downwards instead of upwards. This corresponds to an antivortex. (In a completely ordered region the vorticity will, of course, be zero. Since the vortices appear in "neutral" pairs, if we move around in a large enough path the *net* vorticity will also be zero.) There will of course be other "local" excitations which appear simultaneously so the picture of the lattice will not always be quite so tidy as

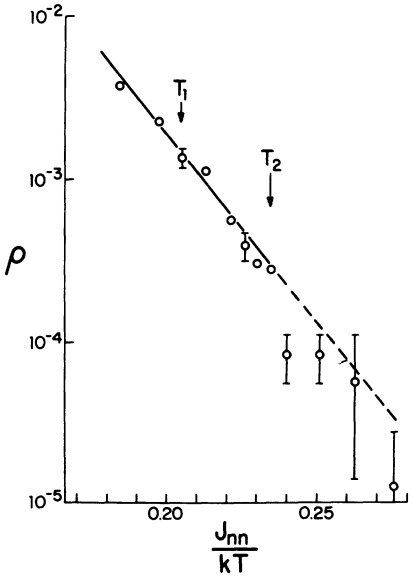

FIG. 12. Temperature dependence of the vortex-pair density in zero field for $R=-1$.

in Fig. 10. In all cases, however, the presence of a "vortex" is signaled by the appearance of an isolated defect triangle. In Fig. 11 we show representations of the lattice at two temperatures showing only isolated defect triangles. At low temperatures relatively few defects (vortices) are present and when they do occur they are in tightly bound vortex-antivortex pairs. As the temperature is increased the number of vortex pairs increases, and at T_1 the pairs begin to unbind. We find that the density of vortex pairs obeys a simple Arrhenius law

$$\rho=\rho_0\exp(-\Delta E/kT)\,, \tag{17}$$

where ΔE is the thermal activation energy for formation of a vortex pair. From Fig. 12 we see that Eq. (17) is valid over a wide range of temperature with $\Delta E=(53\pm 5)J_{\rm NN}$. For comparison we note that the elementary excitation for the $(\sqrt{3}\times\sqrt{3})$ ground state is the addition of a single adatom at a cost in energy of $12\,|J_{\rm NNN}|$. In contrast the removal of a single adatom requires energy $(12J_{\rm NN}+|12J_{\rm NNN}|)$. If we insist that the system remain at 50%, the simplest *local* excitation is the movement of an adatom, i.e., removal of an adatom and the readsorption in another site. Using the values just mentioned, we find that moving an adatom costs in energy $12J_{\rm NN}+24\,|J_{\rm NNN}|$. (Moving it to an unoccupied NN site costs only $10J_{\rm NN}+24\,|J_{\rm NNN}|$.) These excitations are only slightly less energetic than vortex-pair excitation. This situation is quite different in the XY model, where the elementary excitations are spin waves which actually have zero energy at $\vec{k}=0$. For comparison we also note that in the square lattice XY model the vortex-pair creation energy is $\Delta E\sim 6.4J_{\rm NN}$ and in the plane rotator model[22,23] $\Delta E\sim 10J_{\rm NN}$. We see that the "stiffness" of the "vortices" in the present model causes a significant increase in excitation energy (even allowing for the difference in coordination numbers).

3. *Bulk properties for $R\neq -1$*

We have also studied $L=30$ lattices with R varying by 2 orders of magnitude. The specific-heat results for small R are shown in Fig. 13(a). As $R\to 0$, the low-temperature peak shifts rapidly to lower temperatures and the upper peak decreases in magnitude and approaches the rounded maximum which occurs when $R=0$. For large R both peaks shift to higher temperature and it is more illuminating to plot the data versus $kT/|J_{\rm NNN}|$ as shown in Fig. 13(b). The two peaks shift together and begin to approach the single specific-heat peak which occurs when $R=-\infty$, i.e., $J_{\rm NN}=0$, and the system decomposes into two noninteracting NNN Ising triangular ferromagnets. The same qualitative features can be

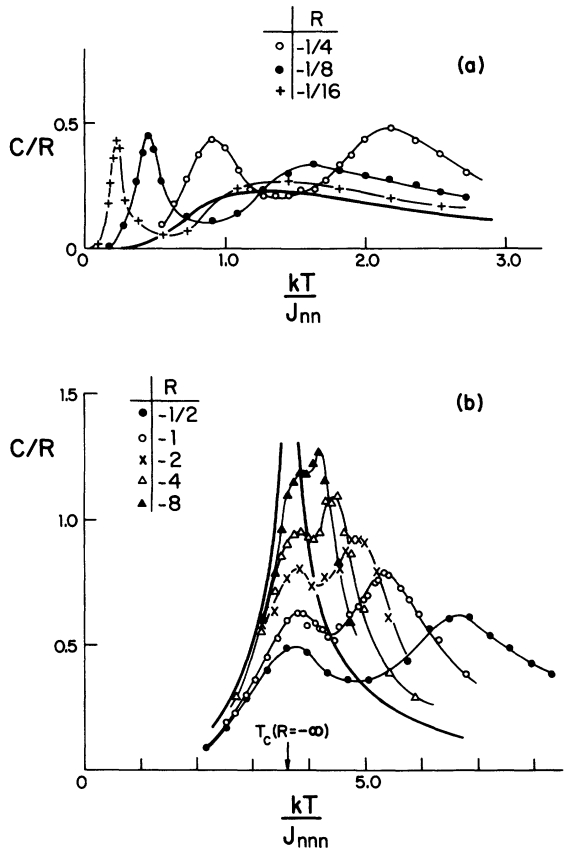

FIG. 13. Temperature dependence of the specific heat for $L=30$ over a wide range of R: (a) $R \geq -\frac{1}{4}$. The heavy solid curve is the exact result for $R=0$. Data are plotted vs kT/J_{NN}. (b) $R \leq -\frac{1}{2}$. The heavy solid curve is the result for $R=-\infty$. Note that the data are plotted vs kT/J_{NNN}.

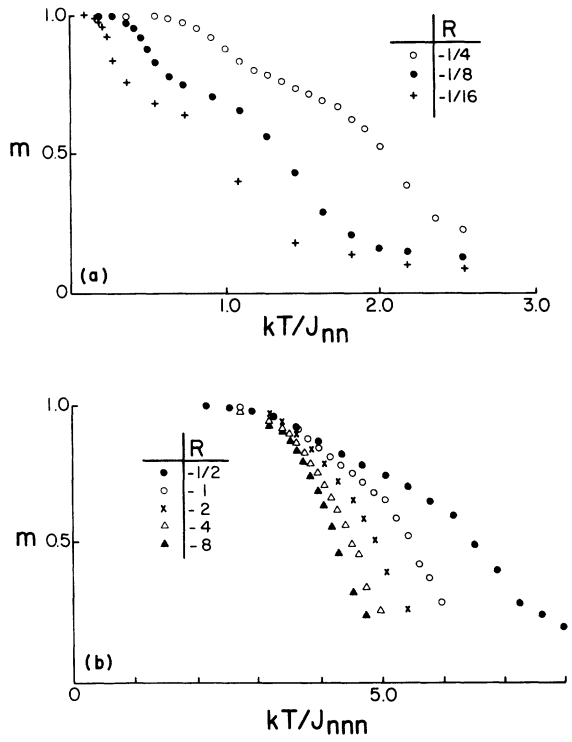

FIG. 14. Temperature dependence of the order parameter for $L=30$: (a) $R \geq -\frac{1}{4}$; (b) $R \leq -\frac{1}{2}$. Note that data in (a) are plotted vs kT/J_{NN} whereas data in (b) are plotted vs kT/J_{NNN}.

seen in the order-parameter results for $L=30$ shown in Fig. 14(a). The finite-lattice behavior becomes particularly interesting for $R > -1$, where the intermediate XY-like region apparently gives rise to a pronounced shoulder in the order parameter. We cannot determine with confidence what happens to T_1 and T_2 as a function of R without doing a detailed finite-size analysis or vortex-pair unbinding search. Both types of analyses are too time consuming for all of the ratios of interactions. Since T_1 and T_2 occur on the low-temperature and high-temperature shoulders of the specific peaks, respectively, for $R=-1$ we may use Fig. 13 to draw some tentative conclusions. As $R \to -\infty$, T_1 and T_2 appear to move towards each other, but we cannot tell if they merge at a finite value of R. For $R > -1$ it appears that T_1 and T_2 first move apart and then begin to approach each other as both approach $T=0$.

B. The ordered phase

1. *Critical behavior*

Since the phase boundaries for $R=J_{NNN}/J_{NN}=-1$ are symmetric about $H=0$, we shall only present results for the $(\sqrt{3}\times\sqrt{3})$ phase. For a wide range of nonzero fields the transition from the ordered to disordered state was continuous. In Fig. 15 we show specific-heat results obtained from a wide range of lattice sizes for $H/J_{NN}=2.43$. These data show a single peak which grows and sharpens as the lattice size is increased. The size dependence of the maximum value of the specific heat is analyzed in Fig. 6. According to finite-size scaling theory the specific-heat peak should diverge as $L^{\alpha/\nu}$; hence the slope of the "fit" shown in Fig. 6 suggests $\alpha/\nu=0.44$. Best estimates for the three-state Potts model[24–26] are $\alpha=\frac{1}{3}$, $\nu=\frac{5}{6}$, or $\alpha/\nu=0.40$. If we subtract off a small negative "background," even the point for $L=12$ will lie on the straight line. For comparison we also show the logarithmically diverging specific-heat peak for the triangular Ising ferromagnet. In Fig. 16 we show

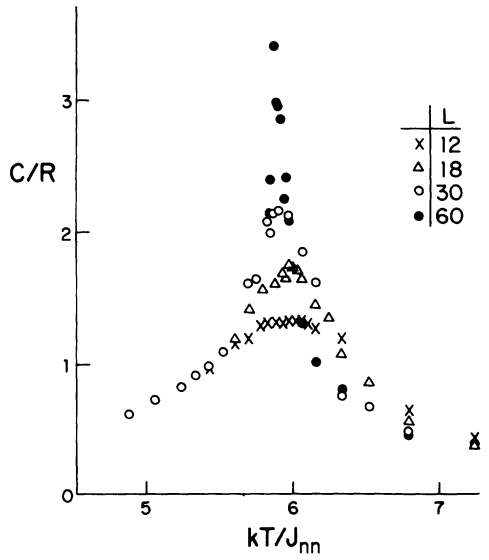

FIG. 15. Specific heat vs temperature for $R=-1$, $H/J_{NN}=2.43$.

log-log plots of the critical behavior of the order parameter and of the high-temperature susceptibility. Finite-size effects are pronounced, but fits to the "asymptotic" behavior suggest $\beta=0.11\pm0.02$, $\gamma=1.42\pm0.12$. These data are reanalyzed in Fig. 17 using finite-size scaling plots. The data scale extremely well using $\beta=0.11$, $\gamma=1.42$, $\nu=0.87$, and the slope for large $x=tL^{1/\nu}$ is consistent with the

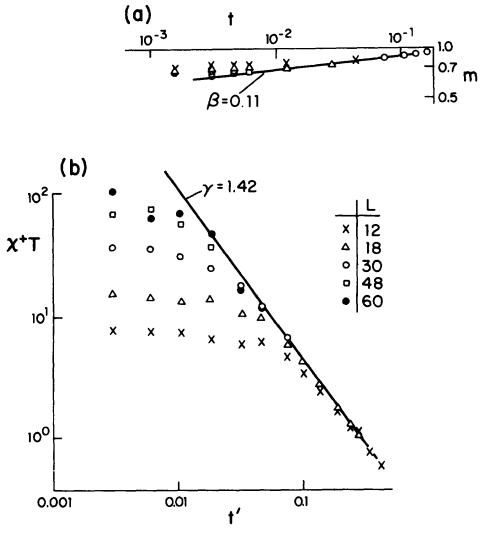

FIG. 16. Critical behavior of the order parameter m and high-temperature ordering susceptibility χ^+ for $R=-1$, $H/J_{NN}=2.43$. $t'=|1-T_c/T|$ and $t=(1-T/T_c)$.

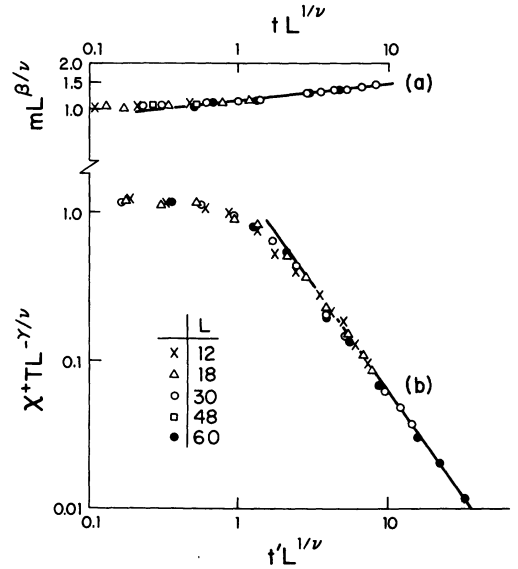

FIG. 17. Finite-size scaling plots for $R=-1$, $H/J_{NN}=2.43$. The plots were made using $\gamma=1.42$, $\beta=0.11$, $\nu=0.87$, $t'=|1-T_c/T|$, and $t=(1-T/T_c)$.

values of β and γ used to make these plots. The values are quite close to "exact" values of $\beta=\frac{1}{9}$, $\gamma=\frac{13}{9}$, $\nu=\frac{5}{6}$. We have also used finite-size scaling to analyze the site-site correlations at T_c. Since $t=0$ at the critical temperature, the finite-size scaling function [see Eq. (12)] depends only upon one scaling variable $y=r/L$. As Fig. 18(b) shows, the data scale quite well with $\eta=0.27$. For comparison we note that the estimate for the three-state Potts model[24] is $\eta=0.266$. We have also analyzed the site-site correlation functions in the NNN direction farther away from T_c assuming a standard Ornstein-Zernike form

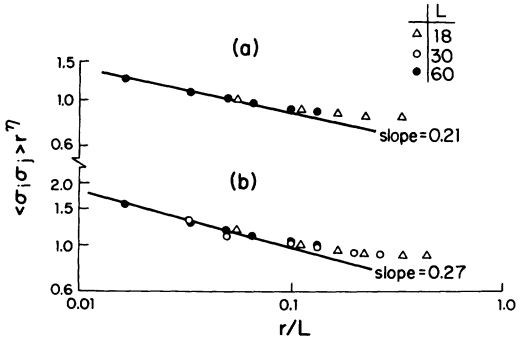

FIG. 18. Finite-size scaling plots for the site-site correlation function along the (11) NNN direction for $R=-1$: (a) "tricritical path" $H/kT=1.26$ with $\eta=0.21$; (b) $H/J_{NN}=2.43$ with $\eta=0.27$. Data are in units of the NNN distance r_{NNN}.

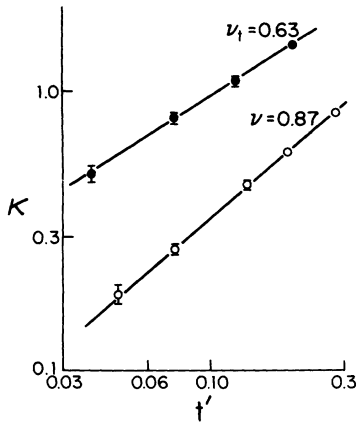

FIG. 19. Critical behavior of the inverse correlation length for $R=-1$. Open circles are data for $H/J_{NN}=2.43$, closed circles are obtained along the "tricritical"path $H/kT=1.26$, $t'=|1-T_c/T|$. Data are in terms of the inverse NNN distance r_{NNN}^{-1}.

$$\langle \sigma_i \sigma_j \rangle = \frac{D \exp(-\kappa r)}{r^{1/2}} , \tag{18}$$

where κ is the inverse correlation length. Using the resultant values of κ we plotted the temperature dependence of κ in Fig. 19. From these data we find $\nu=0.87$ as compared with $\nu=0.833$ predicted from the three-state Potts model.

2. *Critical-degenerate crossover*

For small values of the field the behavior is dominated by crossover from degenerate phase character to critical behavior when the temperature is sufficiently close to T_c. The specific-heat data shown in Fig. 20 show the rapid growth of a sharp peak out of the high-temperature maximum and the disappearance of the low-temperature maximum as the field is slowly increased. The high-temperature ordering susceptibility shows exponential behavior for large values of $t'=|1-T_c/T|$ which becomes power-law-like with $\gamma=1.42\pm0.12$ sufficiently close to T_c (see Fig. 21). We also find that for small fields the variation of the critical temperature can be fit reasonably to

$$H_c/J_{NN}=h_0\exp(-at^{-1/2}) \tag{19}$$

(see Fig. 22). Kinzel and Schick[27] have shown that this kind of exponential variation provides further evidence of an XY-like phase. This behavior means that the phase boundary has a cusp at $H=0$ (see Fig. 23). In Fig. 24 we show the phase diagram in coverage-temperature space. The first-order boundaries open up into large coexistence regions in this diagram. (Qualitative features of this diagram were predicted by den Nijs *et al.*[28]) Although critical exponents usually change as soon as a symmetry-breaking field is introduced and then remain invariant, critical amplitudes associated with the new asymptotic behavior will change continuously. If the critical temperature T_c has a power-law dependence on the field, i.e.,

$$T_c(H)-T_c(0)\propto H^{1/\phi} , \tag{20}$$

the critical amplitudes also have power-law behavior. For example, the susceptibility amplitude C varies as

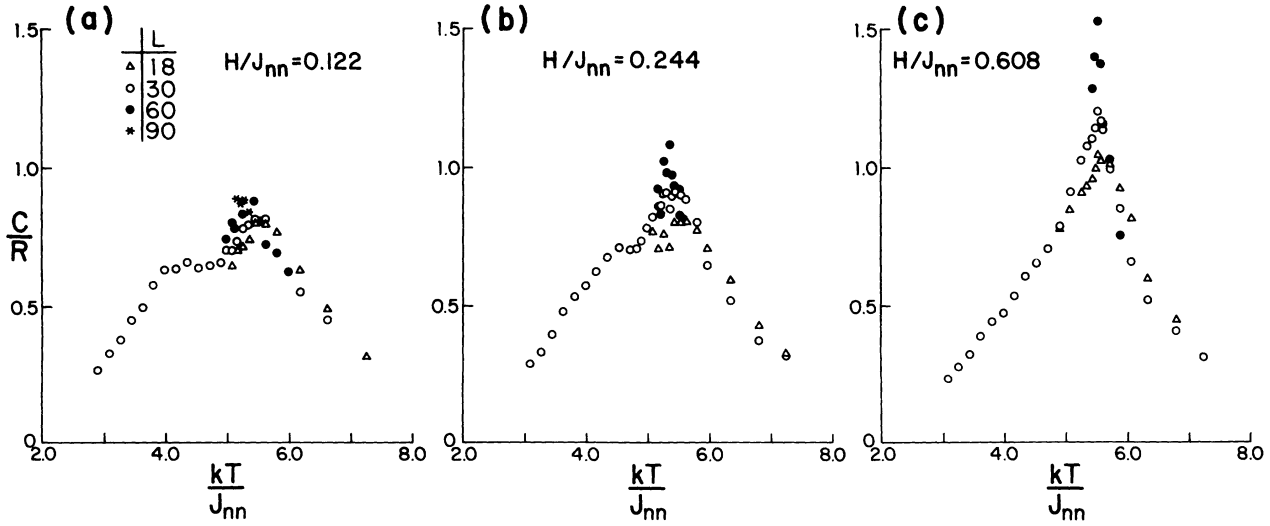

FIG. 20. Specific heat vs temperature along paths of constant field for $R=-1$.

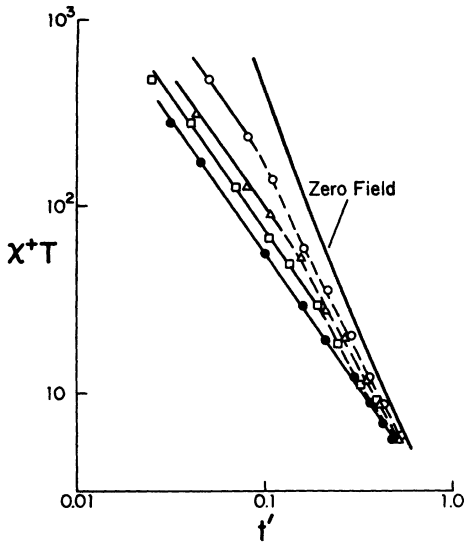

FIG. 21. High-temperature ordering susceptibility along paths of constant field for $R=-1$. Data are for $L=60$ with: ○, $H/J_{NN}=0.122$; △, $H/J_{NN}=0.244$; □, $H/J_{NN}=0.608$; ●, $H/J_{NN}=1.216$. The heavy solid curve shows the result for $H/J_{NN}=0$. Solid straight lines have slope = 1.42.

$$C \propto H^{(\gamma-\gamma_0)/\phi}, \tag{21}$$

where γ_0 is the zero-field exponent and γ the corresponding exponent for $H>0$. If there is instead an exponential singularity then Eqs. (20) and (21) are no longer valid since the exponents are *infinite*. In order to circumvent this difficulty Binder and Landau[29] introduced new critical exponents

$$\tilde{\alpha}=\alpha/\nu,\ \tilde{\beta}=\beta/\nu,\ \tilde{\gamma}=\gamma/\nu,\ \tilde{\phi}=\phi/\nu, \tag{22}$$

which have meaning even if there are exponential singularities. The critical amplitudes are then given by

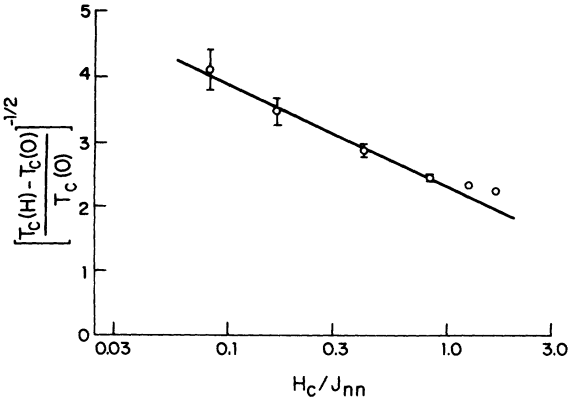

FIG. 22. Variation of the critical temperature $T_c(H)$ with field; $T_c(0)=T_1$.

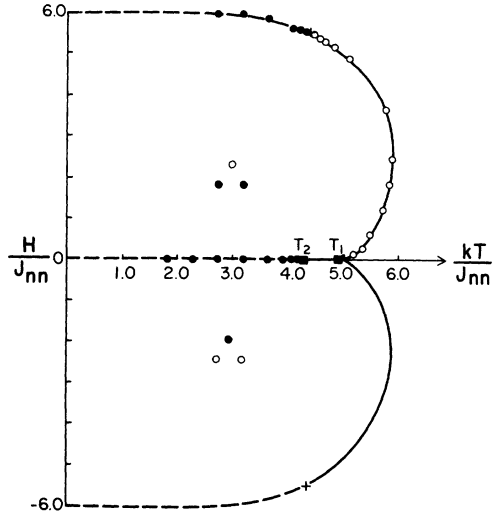

FIG. 23. Phase diagram in the field-temperature plane for $R=-1$. Open circles and solid curves show second-order transitions, and closed circles and dashed lines indicate first-order transitions. Tricritical points are marked by +.

$$A \propto H^{-\tilde{\alpha}/\tilde{\phi}}, \tag{23a}$$

$$B \propto H^{\tilde{\beta}/\tilde{\phi}}, \tag{23b}$$

$$C \propto H^{-\tilde{\gamma}/\tilde{\phi}}, \tag{23c}$$

where the amplitudes are defined in Eq. (11). We have used Eqs. (23) to fit the amplitudes obtained from our data. The data for $H/J_{NN}\leq 1.22$ were consistent with power-law behavior with $\tilde{\alpha}/\tilde{\phi}=0.55\pm0.06$, $\tilde{B}/\tilde{\phi}=0.04\pm0.01$, $\tilde{\gamma}/\tilde{\phi}=0.45\pm0.04$. Using these values, we find that $\tilde{\alpha}+2\tilde{\beta}+\tilde{\gamma}=(0.02\pm0.11)\tilde{\phi}$, which agrees with the modified Rushbrooke relation $\tilde{\alpha}+2\tilde{\beta}+\tilde{\gamma}=0$.

3. *Tricritical behavior*

The behavior of the system near the tricritical point was studied along paths of constant H/kT. This was done so that the paths stayed almost perpendicular to the phase boundary. As the path increases in steepness the asymptotic critical region shrinks in extent, and modified critical behavior appears for larger values of $|T-T_c|$. This is seen clearly in the susceptibility data shown in Fig. 25. Our estimate for the tricritical path is $H/kT=1.26$ and $\gamma_t=1.06\pm0.05$. The tricritical value of β as determined from the order parameter is $\beta_t=0.08\pm0.02$. The theoretical predictions for tricritical exponents of the three-state Potts model[26] are $\gamma_t=1.06$ and $\beta_t=0.06$. The agreement is quite good, especially for γ_t. A finite-size scaling analysis

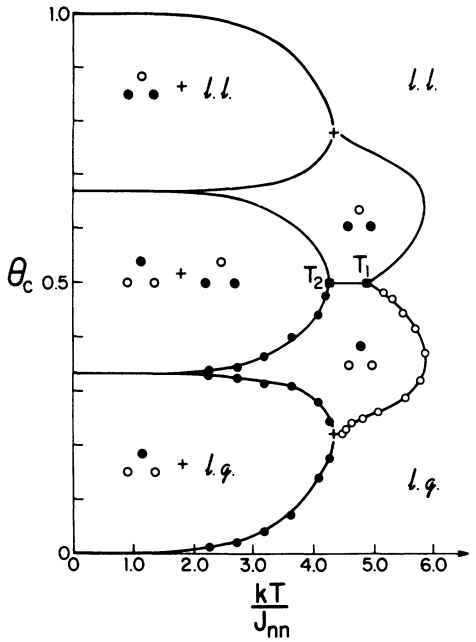

FIG. 24. Phase diagram in the coverage temperature plane for $R=-1$. Open circles show critical magnetizations at second-order transitions and closed circles show the boundaries to coexistence regions. (Data points are only shown for $\theta \leq 0.5$.) l.g. and l.l. refer to lattice-gas and lattice-liquid regions, respectively.

(Fig. 18) of the site-site correlations yields a value of $\eta_t = 0.21 \pm 0.02$. The theoretical prediction for the three-state Potts model[26] is $\eta_t = 0.19$. The difficulty of locating tricritical points in two dimensions because of finite-size metastability effects has been discussed elsewhere.[30] We therefore believe that it is possible that our location of the tricritical point is slightly in error. Our data suggest nonetheless that the tricritical region is so large that our estimates for tricritical exponents should still be reliable. We have also analyzed the site-site correlation functions along the tricritical path above T_t, using the Ornstein-Zernike form. The resultant variation of the inverse correlation length κ with temperature is shown in Fig. 19. κ is in general much larger along the tricritical path than along the critical path. This explains the small finite-size effects. Our estimate of $\nu_t = 0.63 \pm 0.04$ also agrees with the theoretical prediction[26] of $\nu_t = \frac{7}{12} \simeq 0.58$. The finite-size behavior of the specific-heat peak (see Fig. 6) yields $\alpha/\nu = 1.02$ or $\alpha_t = 0.64$. The predicted values are $\alpha_t/\nu_t = \frac{10}{7} \simeq 1.43$ and $\alpha_t = \frac{5}{6} \simeq 0.83$. This discrepancy may be due to a slightly incorrect choice of the "tricritical path" which intersects the phase boundary along the second-order portion just above T_t. It is also possible that the difference is due to the neglect of the background term [see Eq. 11(c)]. The

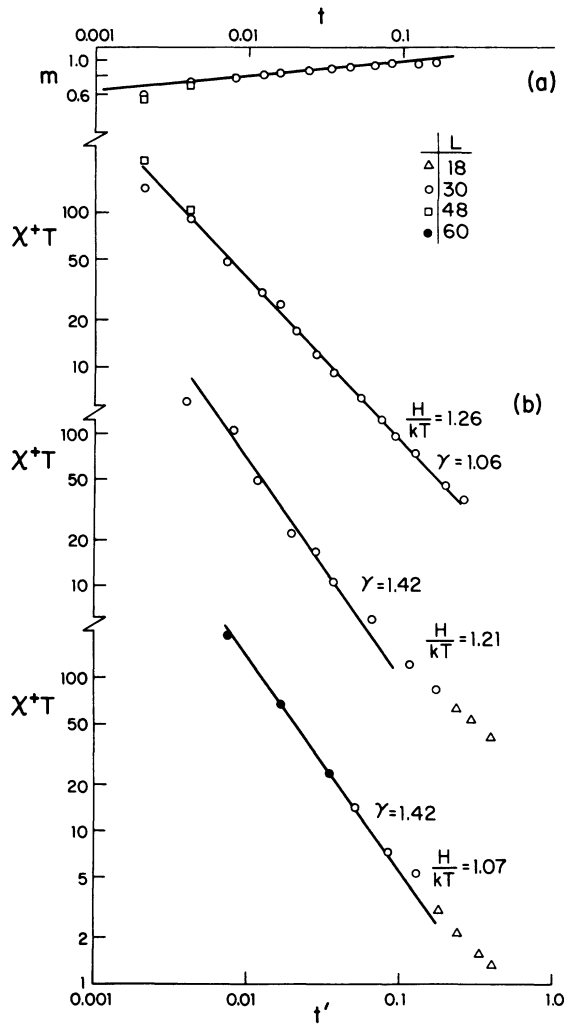

FIG. 25. (a) Critical behavior of the order parameter for $R=-1$ along the tricritical path $H/kT=1.26$; (b) Critical behavior of the high-temperature ordering susceptibility for $R=-1$ along paths of constant H/kT.

density jump exponent which determines how fast $\Delta\theta$ goes to zero at T_t is not in disagreement with the predicted[26] value of $\frac{1}{2}$, however the uncertainty in T_t makes a careful test impossible.

C. Adsorption isotherms

Since properties of adsorbed layers are often determined by measuring adatom coverage versus adsorbate gas pressure, we believe that it is important to show what adsorption isotherms would look like for the present model. In Fig. 26 we plot coverage versus $(\mu+\epsilon)/kT$ for $R=-1$ for different isotherms which show different qualitative behavior according to Fig. 24. The adsorption isotherms are

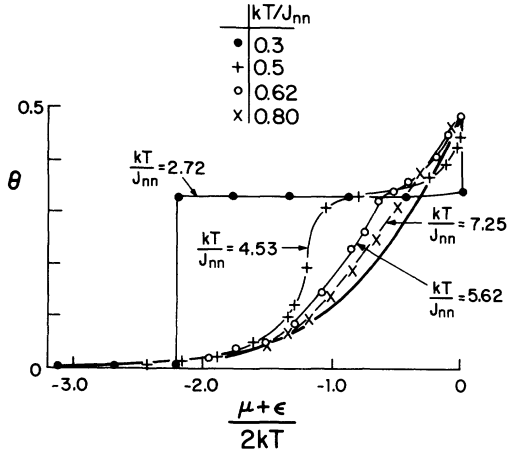

FIG. 26. Adsorption isotherms for $R=-1$. The heavy solid curve is Langmuir's isotherm. The isotherms are antisymmetric about $\theta=0.5$, $(\mu+\epsilon)/kT=0$.

antisymmetric about $\theta_c=\frac{1}{2}$, $\mu+\epsilon=0$. (Note that μ/kT is proportional to the gas pressure if the gas is ideal.) At low temperatures, i.e., below T_2 and T_t, the isotherms show pronounced steps (or risers). These do not correspond to the filling of a monolayer but rather to the filling of a sublattice. As the temperature increases above T_2 and T_t, the risers tend to round off, and the second lowest temperature shown in Fig. 26 ($kT/J_{NN}=4.53$) there are no discontinuous steps. At $kT/J_{NN}=5.62$ the system is initially in the disordered lattice-"gas" state, enters the ordered state and then leaves it again reaching 50% coverage. Note that on this scale it is impossible to determine precisely where the phase transitions occur. At the highest temperature shown, $kT/J_{NN}=7.25$, there is no transition at all and the isotherm looks qualitatively like Langmuir's isotherm.

IV. CONCLUSIONS

Our studies have yielded a rich phase diagram with critical and tricritical behavior which we understand. The exponent values which we have obtained agree well with the predicted exponents for the three-state Potts model and give no indication of the "chiral" behavior suggested by Huse and Fisher.[31] It may be, however, that the effective value of the "chiral field" is small enough for our model so that the transition remains in the Potts universality class. It is also possible that the chiral exponents are very close to those of the three-state Potts model and that we cannot distinguish between the two with the resolution available to us. Although we believe that the tricritical points as well as T_1 and T_2 move continuously to $T=0$ as $R\to 0$, we do not yet have direct evidence to support this idea. Since no "crossover" occurs when $R=0$ which for $T\to 0$ gives hard hexagons, i.e., simple Potts exponents, it is also possible that $T_t\to 0$ for some nonzero R.[32] Interpreting the data at 50% coverage to extract the correct $L=\infty$ critical behavior is a difficult and somewhat confusing task. For example, our conclusions differ noticeably from those drawn recently by Wada *et al.*[33] and Fujiki *et al.*[34] based on less extensive data. We do not believe that the methods used in this paper will be fruitful for studying the small-R behavior for 50% coverage because of the vast amount of data needed to carry out the finite-size analyses. Since adsorption of noble gases on graphite does not extend to a registered, $\theta=0.5$ phase, experimental results on other substrates with the same symmetry are needed in order to determine the applicability of the present model to physical systems. Another possibility would be to study compositional ordering of krypton-xenon mixtures or graphite; den Nijs *et al.*[28] have suggested that this system should have an equivalent phase diagram.

ACKNOWLEDGMENTS

We are deeply indebted to R. B. Griffiths, M. Schick, and R. H. Swendsen for many illuminating discussions and suggestions. We also wish to thank M. E. Fisher and M. P. Nightingale for helpful comments about the manuscript. This research was supported in part by National Science Foundation—Condensed Matter Theory Program Grant No. DMR-79-26178.

[1]See M. E. Fisher, Rep. Prog. Phys. 30, 615 (1967) for both discussion of this equivalence and references to earlier work on this topic.

[2]G. H. Wannier, Phys. Rev. 79, 357 (1950); R. M. F. Houtappel, Physica 16, 425 (1950).

[3]B. D. Metcalf, Phys. Lett. 45A, 1 (1973).

[4]M. Schick, J. S. Walker, and M. Wortis, Phys. Rev. B 16, 2205 (1977).

[5]Since occupied sites correspond to Ising spin up and unoccupied sites to Ising spin down, the $(\sqrt{3}\times\sqrt{3})$ and $(\sqrt{3}\times\sqrt{3})^*$ states correspond simply to the time reversed ferrimagnetic states in which $\frac{2}{3}$ of the spins

point in one direction and $\frac{1}{3}$ point in the opposite direction.

[6]C. E. Campbell and M. Schick, Phys. Rev. A 5, 1919 (1972).

[7]See, e.g., A. N. Berker, S. Ostlund, and F. A. Putnam, Phys. Rev. B 17, 3650 (1978), and references therein.

[8]See R. J. Birgeneau, E. M. Hammons, P. Heiny, P. W. Stephens, and P. M. Horn, in *Ordering in Two Dimensions,* edited by S. K. Sinha (Elsevier, New York, 1980).

[9]S. Alexander, Phys. Lett. 54A, 353 (1975).

[10]E. Domany, M. Schick, J. S. Walker, and R. B. Griffiths, Phys. Rev. B 18, 2209 (1978). See also S. Alexander and P. Pincus, J. Phys. A 13, 263 (1980).

[11]B. Mihura and D. P. Landau, Phys. Rev. Lett. 38, 977 (1977).

[12]J. V. José, L. P. Kadanoff, S. Kirkpatrick, and D. R. Nelson, Phys. Rev. B 16, 1217 (1977).

[13]S. Elitzur, R. B. Pearson, and J. Shigemitsu, Phys. Rev. D 19, 3698 (1979).

[14]K. Binder and D. P. Landau, Surf. Sci. 61, 577 (1976); Phys. Rev. B 21, 1941 (1980).

[15]M. E. Fisher, in *Proceedings of the International Summer School "Enrico Fermi" 1970, Course, 51,* Varrena, Italy, edited by M. S. Green (Academic, New York, 1971).

[16]The correctness of finite-size scaling theory has been verified for a variety of Ising models. See, for example, Refs. 17 and 18.

[17]A. E. Ferdinand and M. E. Fisher, Phys. Rev. 185, 832 (1969).

[18]D. P. Landau, Phys. Rev. B 14, 255 (1969); 13, 2997 (1976); 14, 255 (1976); 16, 4164 (1977).

[19]J. M. Kosterlitz and D. J. Thouless, J. Phys. C 6, 1181 (1973).

[20]K. Binder, in *Monte Carlo Methods in Statistical Physics,* edited by K. Binder (Springer, Berlin, 1979).

[21]D. P. Landau, J. Appl. Phys. 42, 1284 (1971).

[22]D. P. Landau and K. Binder, Phys. Rev. B 24, 1391 (1981).

[23]J. Tobochnik and G. V. Chester, Phys. Rev. B 20, 3761 (1979).

[24]Exponent estimates for the critical and tricritical behavior are obtained from Baxter's result (Ref. 25) for the hard hexagon model (which should be in the same universality class) and a series of conjectures (Ref. 26) which are correct for every case where a check is available.

[25]R. J. Baxter, J. Phys. A 13, L61 (1980).

[26]M. P. M. den Nijs, J. Phys. A 12, 1857 (1979); B. Nienhuis, A. N. Berker, E. K. Riedel, and M. Schick, Phys. Rev. Lett. 43, 737 (1979); R. B. Pearson, Phys. Rev. B 22, 2579 (1980); J. L. Black and V. J. Emery, *ibid.* 23, 429 (1981); B. Nienhuis, J. Phys. A 15, 199 (1982); M. P. M. den Nijs (unpublished).

[27]W. Kinzel and M. Schick, Phys. Rev. B 23, 3435 (1981).

[28]M. P. M. den Nijs, M. P. Nightingale, and M. Schick, Phys. Rev. B 26, 2490 (1982).

[29]K. Binder and D. P. Landau, Phys. Rev. B 13, 1140 (1976).

[30]D. P. Landau and R. H. Swendsen, Phys. Rev. Lett. 46, 1437 (1981).

[31]D. A. Huse and M. E. Fisher, Phys. Rev. Lett. 49, 793 (1982).

[32]M. E. Fisher (private communication).

[33]K. Wada, T. Tsukada, and T. Ishikawa, J. Phys. Soc. Jpn. 51, 1331 (1982).

[34]S. Fujiki, K. Shutoh, Y. Abe, and S. Katsura (unpublished).